Int j simul model 13 (2014) 3, 312-322
ISSN 1726-4529 Original scientific paper

LAMINAR FORCED CONVECTION HEAT TRANSFER CHARACTERISTICS FROM A HEATED CYLINDER IN WATER BASED NANOFLUIDS

Ternik, P.[*] & Rudolf, R.[**,***]

[*] Ternik Primoz – Private Researcher, Bresterniska 163, 2354 Bresternica, Slovenia
[**] University of Maribor, Faculty of Mechanical Engineering, Smetanova 17, 2000 Maribor, Slovenia
[***] Zlatarna Celje d.d., Kersnikova 19, 3000 Celje, Slovenia
E-Mail: pternik@pt-rtd.eu, rebeka.rudolf@um.si

Abstract
Forced convection heat transfer from a heated circular cylinder to incompressible water-based nanofluids in the steady cross-flow regime has been investigated numerically. The momentum and thermal energy differential equations have been solved by the standard finite volume method on the non-uniform Cartesian grid.

The main objective of this study is to investigate the influence of the nanoparticles' volume fraction ($0\ \% \le \varphi \le 10\ \%$) on the heat transfer characteristics of water-based nanofluids over a wide range of base-fluid Reynolds number ($1 \le \mathrm{Re}_{bf} \le 20$).

Accurate numerical results are presented in the form of the local and mean Nusselt number and the heat transfer enhancement. The results indicate clearly that the heat transfer characteristics are affected by the base-fluid Reynolds number, volume fraction and the thermo-physical properties of nanoparticles. Although those nanofluids reduce the mean Nusselt number values, they enhance the heat transfer rate.
(Received in November 2013, accepted in March 2014. This paper was with the authors 1 month for 1 revision.)

Key Words: Laminar Flow, Circular Cylinder, Nusselt Number, Heat Transfer Rate Enhancement, Numerical Modelling

1. INTRODUCTION

Due to the unique properties of nanoparticles and possibilities of their use in daily life, nanotechnology is experiencing an unprecedented growth in recent years [1]. In many industrial applications such as power generation, microelectronics, heating processes, cooling processes and chemical processes, water, mineral oil and ethylene glycol are used as heat transfer fluid. Effectiveness and high compactness of heat exchangers are obstructed by the lower heat transfer properties of these common fluids as compared to most solids. It is obvious that solid particles having thermal conductivities several hundred times higher than these conventional fluids must be used in the heat transfer applications. To improve thermal conductivity of a fluid, suspension of ultrafine solid particles in the fluid can be a creative idea. For that, nanosized particles dispersed in a base fluid, known as nanofluid, have been used and researched extensively to enhance the heat transfer. Many of the researchers have studied the heat transfer characteristics of nanofluids in the last decade experimentally as well as computationally. There have been concerns if the nanofluids can be studied as a single-phase fluid or they have to be treated as a two-phase mixture [2]. Although they are more accurate in predicting heat transfer, two-phase models [3, 4] are computationally more expensive than the single-phase models due to the increased number of equations to be solved. Use of the single-phase model for nanofluids simplifies the application of computational fluid dynamics as only the material properties in governing equations need to be modified with appropriate correlations and this simplicity has attracted the attention of researchers for investigating the flow and heat transfer behaviour of various nanofluids.

Natural convection in nanofluids is one of the most extensively analyzed configurations because of its relevance in various engineering systems [5, 6]. To date, most of the authors (e.g. [7, 8]) claim that the presence of nanoparticles in a fluid alters the flow structure and increases the natural convection mean Nusselt number for any given characteristic (i.e. *Ra* or *Gr*) number. On the other hand, an apparently paradoxical behaviour of heat transfer deterioration was observed in experimental studies. For example, Putra et al. [9] reported that the presence of Al_2O_3 and CuO nanoparticles in a base-fluid reduce the Nusselt number for the natural convection inside a horizontal cylinder heated from one end and cooled from the other. However, they did not explain clearly why natural convective heat transfer is decreased with an increase in volume fraction of nanoparticles. This was later explained by the recent works of Ternik et al. [10] and Ternik and Rudolf [11]. By utilizing the appropriate expression for the mean Nusselt number they showed that the mean Nusselt number values obtained for the water-based nanofluids are smaller than those obtained in the case of the pure base-fluid at the same nominal values of the base-fluid Rayleigh number. Furthermore, the increasing trend of Nusselt number (as observed by most of the authors) was attributed to the use of the ratio of the nanofluid to the base-fluid thermal conductivity (k_{nf}/k_{bf}) in a definition of the nanofluid Nusselt number.

On the other hand, as far as known to us, there is only limited number of studies on forced convection heat transfer from heated cylinders to nanofluids. Valipour and Zare Ghadi [12] performed numerical study on fluid flow and heat transfer in nanofluid around a circular cylinder. Their results showed that as the solid volume fraction increases, the magnitude of minimum velocity in the wake region and recirculation length increases but separation angle decreases. A study on unconfined nanofluid flow and heat transfer around a square cylinder has been performed by Etminan-Farooji et al. [13]. They focused more on the effects of Peclet number and types of nanofluids on heat transfer from the cylinder rather than fluid flow hydrodynamics. Sarkar et al. [14] studied vortex structure distributions and mixed convective heat transfer around a solid circular cylinder utilizing nanofluid for unsteady regime. Their result showed that the Strouhal number increases by increasing solid volume fraction. They also showed that increase in Strouhal numbers leads to reduction in vortex detachment.

The above review of the existing literature shows that the problem of forced convection heat transfer in nanofluids from unbounded heated circular cylinder at low Reynolds number is an issue still far from being completely solved. In addition to the academic interest, such a structure has also the tremendous engineering applications [15-19]. Framed in this general background, the purpose of the present study is to perform a comprehensive numerical study to investigate the laminar forced convection heat transfer around a heated circular cylinder using nanofluids.

The rest of the paper is organised as follows. The necessary mathematical background and numerical details are presented Section 2 and Section 3 which is followed by the grid refinement, numerical accuracy assessment and validation study (Section 4). Following this analysis, the results are presented and subsequently discussed (Section 5). The main findings are summarised and conclusions are drawn in the final section of this paper.

2. NUMERICAL MODELLING

The standard finite volume method is used to solve the coupled conservation equations of mass, momentum and energy. In the present framework, the second-order central differencing scheme is used for the diffusive terms and the second-order upwind scheme for the convective terms. The convergence criteria were set to 10^{-9} for all the relative (scaled) residuals.

2.1 Governing equations

For the present study steady-state flow of an incompressible water based nanofluids is considered. It is assumed that the fluid phase and nanoparticles are in both, thermal and chemical equilibrium, and there is no slip between them. Except for the density the properties of nanoparticles and fluid are taken to be constant (Table I).

Table I: Thermo-physical properties of water based nanofluids.

	ρ [kg / m^3]	c_p [J / kgK]	k [W / mK]	β [1 / K]
Water	997,1	4179	0,613	$2{,}1\times10^{-4}$
Au	19320	128,8	314,4	$1{,}416\times10^{-7}$
Al_2O_3	3970	765	40	$8{,}5\times10^{-6}$
Cu	8933	385	400	$1{,}67\times10^{-5}$
TiO_2	4250	686,2	8,9538	$9{,}0\times10^{-6}$

The governing equations (mass, momentum and energy conservation) for a steady, laminar and incompressible flow are:

$$\frac{\partial v_i}{\partial x_i} = 0 \tag{1}$$

$$\rho_{nf} v_j \frac{\partial v_i}{\partial x_j} - \frac{\partial}{\partial x_j}\left[\eta_{nf}\frac{\partial v_i}{\partial x_j}\right] = -\frac{\partial p}{\partial x_i} + \frac{\partial}{\partial x_j}\left[\eta_{nf}\frac{\partial v_j}{\partial x_i}\right] \tag{2}$$

$$\left(\rho c_p\right)_{nf} v_j \frac{\partial T}{\partial x_j} = \frac{\partial}{\partial x_j}\left(k_{nf}\frac{\partial T}{\partial x_j}\right) \tag{3}$$

Relationships between properties of nanofluid (nf) to those of base fluid (bf) and pure solid (s) are given with the following empirical models [10, 11]:

- Density: $\rho_{nf} = (1-\varphi)\rho_{bf} + \varphi\rho_s$
- Dynamic viscosity: $\eta_{nf} = \eta_{bf} / (1-\varphi)^{2.5}$
- Thermal expansion: $(\rho\beta)_{nf} = (1-\varphi)(\rho\beta)_{bf} + \varphi(\rho\beta)_s$
- Heat capacitance: $\left(\rho c_p\right)_{nf} = (1-\varphi)\left(\rho c_p\right)_{bf} + \varphi\left(\rho c_p\right)_s$
- Thermal conductivity: $k_{nf} = k_{bf}\dfrac{k_s + 2k_{bf} - 2\varphi\left(k_{bf} - k_s\right)}{k_s + 2k_{bf} + \varphi\left(k_{bf} - k_s\right)}$

2.2 Geometry and boundary conditions

The problem of the slowly moving flow of nanofluids past a stationary circular cylinder of radius R placed symmetrically between parallel plates is schematically depicted in Fig. 1. The full length of computational domain is $L_x = 61\,R$ and the height is $L_y = 30{,}5\,R$.

Only half of the domain is used for the present computations, with the symmetry boundary conditions (zero normal gradients for all variables and zero normal velocity components) imposed along the longitudinal mid-plane. For the slowly moving flow conditions (as investigated in the present study) it is our belief that this is a reasonable modelling assumption.

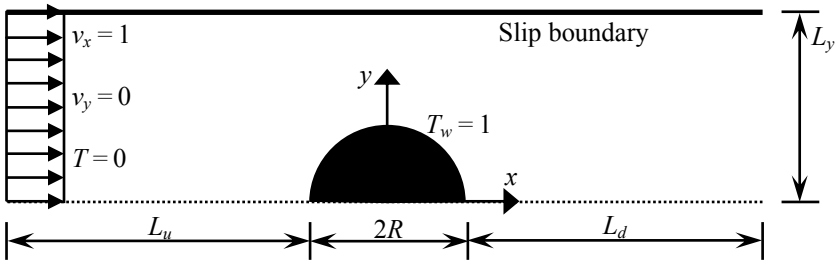

Figure 1: Schematic representation of geometry.

Block-structured meshes were generated with a subdivision of the fluid flow domain into five blocks. Computational meshes used in the present study are non-uniform to allow local refinement, i.e. within particular block the computational cells were concentrated in the radial direction of the cylinder surface. In total, four computational meshes with constant grid refinement (along cylinder surface) were used in the present study.

At the outflow boundary, where the clear region of fully developed flow is re-established by considering the sufficient length of the downstream section, we impose the well known and almost universally used boundary conditions in the finite volume method [20], i. e. vanishing axial variation of the velocity components and temperature, and fixed value for the pressure. The latter (obtaining the pressure field inside the domain by specifying the reference value) is a common practice since the pressure field obtained by solving the pressure-correction equation does not give absolute pressures [21].

In the present study, the heat transfer characteristics are presented (and compared for the same value of the nanofluid Reynolds number) in terms of the local Nusselt number on the surface of circular cylinder:

$$Nu_{nf}(\theta) = \frac{h_{nf} D}{k_{nf}} = -\frac{\partial T}{\partial n_s} \tag{4}$$

Such local values have been further averaged over the surface of a cylinder to obtain the surface averaged (or overall mean) Nusselt number as follows:

$$\overline{Nu} = \frac{1}{2\pi}\int_0^{\pi} Nu(\theta) d\theta \tag{5}$$

In order to investigate the influence of solid particles volume fraction φ on the heat transfer characteristics, the Reynolds and Prandtl number of the nanofluids can be expressed as:

$$\mathrm{Re}_{nf} = \frac{\rho_{nf}}{\rho_{bf}}\frac{\eta_{bf}}{\eta_{nf}}\mathrm{Re}_{bf}, \quad \mathrm{Pr}_{nf} = \frac{\eta_{nf}}{\eta_{bf}}\frac{c_{p,nf}}{c_{p,bf}}\frac{k_{bf}}{k_{nf}}\mathrm{Pr}_{bf} \tag{6}$$

Using eq. (6) we show (Fig. 2) that value of the nanofluid Prandtl number decreases as the volume fraction of nanoparticles in the base-fluid is increased. On the other hand, addition of solid nanoparticles to the base-fluid increases the nanofluid Reynolds number. It is interesting to notice that Au nanoparticles are characterized by the biggest decrease in Pr_{nf} values and biggest increase in Re_{nf} values.

3. NUMERICAL METHOD

The governing equations were solved by taking the advantage of the open-source OpenFOAM CFD software package which employs the standard finite volume method. It is written in C++ and uses classes and templates to manipulate and operate scalars, vectorial and tensorial fields [22]. The advantages of using OpenFOAMas a CFD framework are that the software is freely

available (with open source, licensed under GNU General License Software) and both flexible and highly extensible. Its hierarchical, open structure allows the user to make transparent modifications to the governing equations being solved, to tailor them to specific applications whilst retaining the benefits of a stable and general numerical framework.

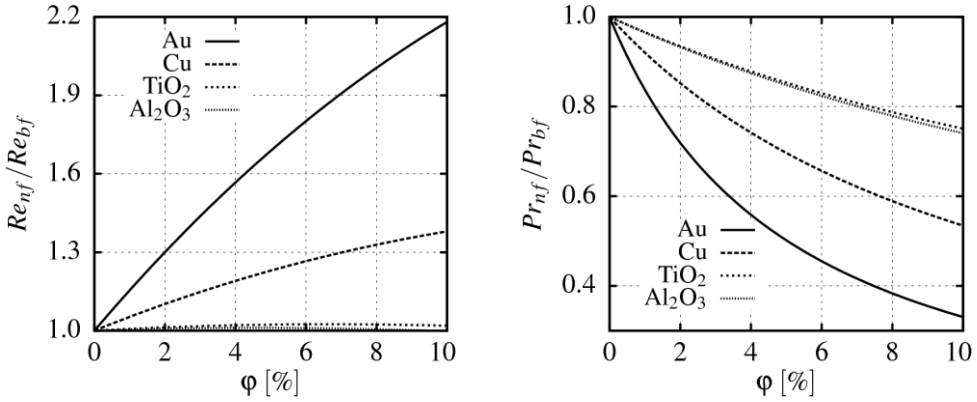

Figure 2: Variation of Reynolds number (left) and Prandtl number (right) with the volume fraction of nanoparticles.

Each governing equation is discretized in a space by integration over the set of control volumes forming the computational mesh. Such a process results in a system of linearized equations of mass, momentum and temperature conservation joined with the constitutive equation. In these equations all variables are evaluated (and stored) in the centre of control volumes populating the physical domain being considered.

The steady incompressible solver SimpleFoam (version 2.1.1) has been modified and used for the present study; governing equations were solved in a segregated manner, followed by the SIMPLE pressure‑velocity correction loop [23]. For solving the linear systems of equations a preconditioned conjugate gradient schemes have been used for velocity, temperature and pressure. All, velocity, temperature, and pressure equations were solved to tolerances 10^{-8}.

In spite of some compelling features of finite volume method (e.g. resulting solutions satisfies the conservation of quantities such as mass, momentum, etc.) there are some undesirable numerical effects (for example, artificial diffusion [20]) that are influenced by the low-order interpolation of the convection terms in governing equations. In order to overcome those undesirable numerical effects, the second-order accurate linear upwind differencing scheme [24] was used in the present study.

4. GRID REFINEMENT, NUMERICAL ACCURACY AND VALIDATION

The aim of most (if not all) numerical analysis is to achieve a certain accuracy with the smallest amount of a computational work. The difficulty to accomplish this usually lies in the unknown behaviour of the flow under numerical investigation. The influence of computational grid refinement on numerical results was examined throughout the examination of spatial (grid) convergence. For this the nanofluid fluid flow ($Re_{bf} = 20$, $\varphi = 0$ %) was studied using four computational meshes.

With each grid refinement the number of control volumes in particular direction is doubled and minimum element size is halved. Such a procedure is useful and encountered in many numerical studies [25-28] for applying the Richardson's extrapolation technique which is a method for obtaining a higher-order estimate of the flow value (value at infinite grid) from a series of lower-order discrete values.

For a general primitive variable ϕ the grid-converged (i.e. extrapolated to the zero element size) value according to Richardson extrapolation is given as:

$$\phi_{ext} = \phi_{MIII} - \left(\phi_{MII} - \phi_{MIII}\right) \Big/ \left(r^p - 1\right) \tag{7}$$

where ϕ_{MIII} is obtained on the finest grid and ϕ_{MII} is the solution based on next level of coarse grid, r = 2 is ratio between the coarse to fine grid spacing and p = 2 is the order of convergence.

Table II: Effect of mesh refinement on the mean Nusselt number for water-Au nanofluid (Re_{bf} = 20, φ = 0 %).

	MI	*MII*	*MIII*	*MIV*	$\overline{Nu}_{ext}$	*Error*
Num. el.	6000	24000	96000	384000	/	/
$\overline{Nu}$	5,141	5,114	5,106	5,103	5,102	0,07 %

The variation of the mean Nusselt number $\overline{Nu}$ with the grid refinement is provided in tabulated form in Table II. The "percent" numerical error for the mean Nusselt number:

$$Error = \left| \left(\overline{Nu}_{MIII} - \overline{Nu}_{ext}\right) \Big/ \overline{Nu}_{ext} \right| \times 100\% \tag{8}$$

as given in Table II is a quantification of the relative difference between the numerical predictions of $\overline{Nu}$ on *MIII* and the extrapolated value $\overline{Nu}_{ext}$ obtained from Richardson's extrapolation technique. It can be seen that the differences with grid refinement are exceedingly small and the agreement between mesh *MIII* and extrapolated value is extremely good; the discretisation error for $\overline{Nu}$ is less than 0,1 %.

In addition to the aforementioned grid-dependency study, the present simulation results have also been compared against the available results of other authors [29, 30] for the forced convection in Newtonian fluid from heated circular cylinder. The comparisons between the present numerical results (obtained with mesh *MIII*) with the benchmark values (summarised in Table III) are extremely good and entirely consistent with our grid-dependency studies.

Table III: Comparison of the present results with the benchmark values (Pr = 1).

	$Re = 5$ $\overline{Nu}$	$Re = 10$ $\overline{Nu}$	$Re = 20$ $\overline{Nu}$
Present study	1,578	2,073	2,748
Bharti et al. [28]	1,586	2,087	2,772
Soares et al. [29]	1,590	2,058	2,696

All these results and comparison with existing numerical data from the literature gave sufficient confidence in the present numerical procedure allowing us to proceed with simulations over the whole range of Re_{bf} and φ. Accounting for numerical accuracy and number of elements mesh *MIII* was found to be a fair compromise and all results presented in continuation were obtained with this mesh.

5. RESULTS AND DISCUSSION

The dependence of the local Nusselt number $Nu(\Theta)$ on the surface of the cylinder and of the average Nusselt number $\overline{Nu}$ on the nanoparticles' volume fraction and type of nanoparticles is presented and discussed in the ensuing sections.

5.1 Variation of local Nusselt number on the surface of the cylinder

Figs. 3 and 4 show the representative variation of the local Nusselt number $Nu(\Theta)$ on the surface of the cylinder with the nanoparticles' volume fraction φ for all nanofluids studied. While these figures show qualitatively similar behaviour of the local Nusselt number over the surface of the cylinder, a complex interplay between the volume fraction and base-fluid Reynolds number is observed in quantitative terms.

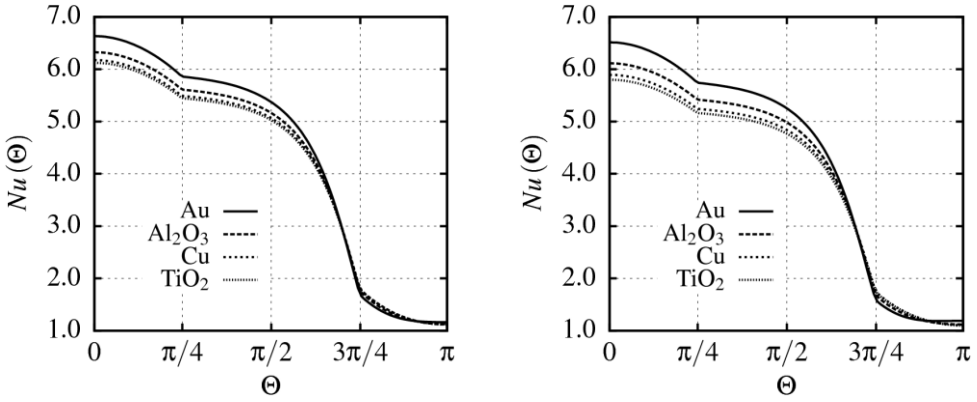

Figure 3: Variation of the local Nusselt number over the surface of the cylinder at $Re_{bf} = 10$ for $\varphi = 5$ % (left) and $\varphi = 10$ % (right).

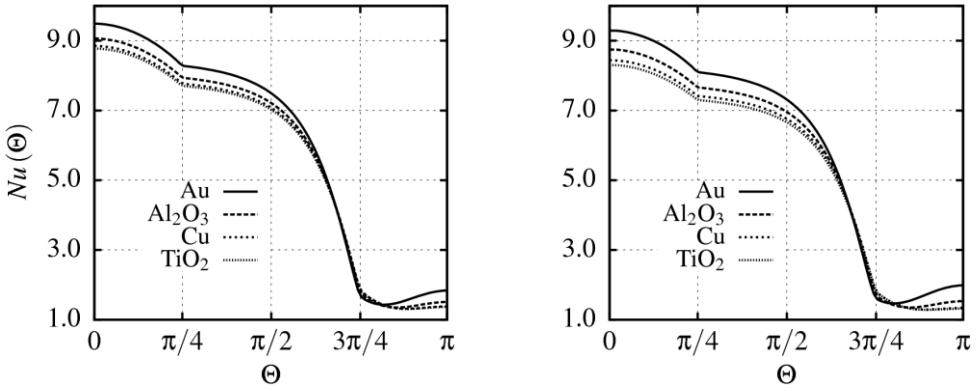

Figure 4: Variation of the local Nusselt number over the surface of the cylinder at $Re_{bf} = 20$ for $\varphi = 5$ % (left) and $\varphi = 10$ % (right).

Value of the local Nusselt number increases with an increase in the base-fluid Reynolds number, but on the other hand it decreases with an increase in the nanoparticles' volume fraction. The latter is a reflection of the fact that addition of nanoparticles to the base-fluid decreases the nanofluid Prandtl number and increases the thermal diffusivity, which causes the reduction in the temperature gradients and, accordingly, increases the thermal boundary thickness. Finally, this increase in the thermal boundary layer thickness reduces the local Nusselt number values.

For lower values of the base-fluid Reynolds number, the local Nusselt number decreases from the front of the cylinder all the way up to the rear of the cylinder, because there is no flow separation (Fig. 3). As the base-fluid Reynolds number increases, the increase in the local Nusselt number can be observed in the vicinity of the rear stagnation point (Fig. 4) due to the occurrence of recirculating region (flow separation).

5.2 Mean Nusselt number

Fig. 5 presents the variation of the mean Nusselt number along the heated wall of circular cylinder. As expected, the mean Nusselt number increases as the base-fluid Reynolds number increases for a given value of the nanoparticles' volume fraction.

On the other hand (and as for the natural convection of nanofluids [10, 11, 25, 27]), one can observe that adding nanoparticles to the base-fluid results in a decrease of the mean Nusselt number values for a given value of the base-fluid Reynolds number. This is due to the fact that addition of nanoparticles to the base-fluid decreases the nanofluid Prandtl number (as shown in Fig. 2 right) and entirely consistent with the earlier findings in the context of the forced convection of generalized Newtonian fluids from a heated cylinder [29].

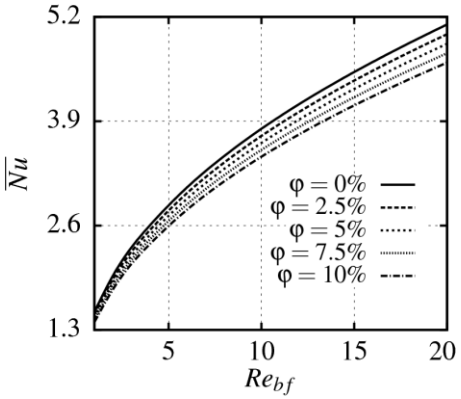

Figure 5: Variation of the mean Nusselt number $\overline{Nu}$ with volume fraction φ and base-fluid Reynolds number Re_{bf} for water-based Al_2O_3 nanofluid.

The variation of the mean Nusselt number $\overline{Nu}$ with the base-fluid Reynolds number Re_{bf} for all water-based nanofluids considered in the present study is shown in Fig. 6 which indicates that $\overline{Nu}$ increases monotonically with an increasing Re_{bf}. Considering the type of nanoparticles, Au and Cu water-based nanofluid is characterized with the highest values of the mean Nusselt number.

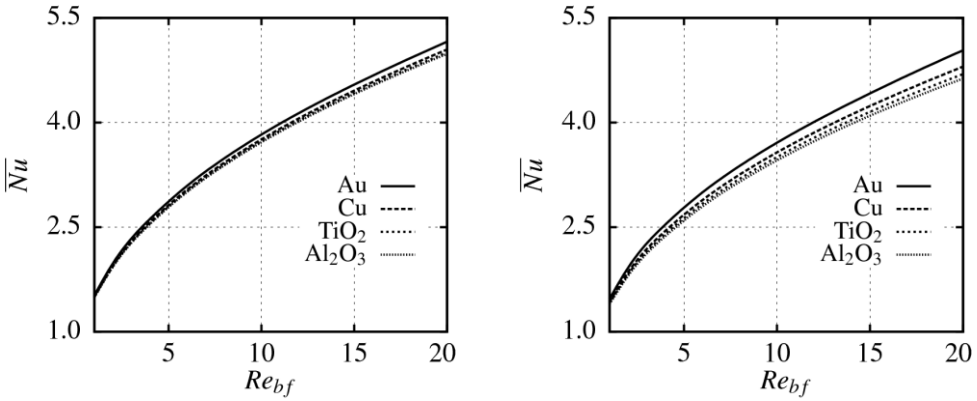

Figure 6: Variation of the mean Nusselt number $\overline{Nu}$ with the base-fluid Reynolds number Re_{bf} for water-based nanofluids at $\varphi = 2{,}5$ % (left) and $\varphi = 10$ % (right).

5.3 Heat transfer rate enhancement

The relative enhancement of the heat transfer rate E [11, 26]:

$$E = \frac{Q_{nf} - Q_{bf}}{Q_{bf}} \times 100\% = \left[\frac{k_{nf}}{k_{bf}} \frac{\overline{Nu}_{nf}}{\overline{Nu}_{bf}} - 1 \right] \times 100\% \tag{9}$$

of the studied water-based nanofluids is plotted in Fig. 7 for two values of the nanoparticles' volume fraction. Considering the base-fluid Reynolds number, the Fig. 7 illustrates that enhancement of the heat transfer rate increases with increasing Re_{bf} for Au and Cu water-based nanofluids, while for Al_2O_3 and TiO_2 one can observe a slight decrease in E as Re_{bf} increases. Furthermore, Fig. 7 presents that the heat transfer enhancement increases with an increase in nanoparticles' volume fraction.

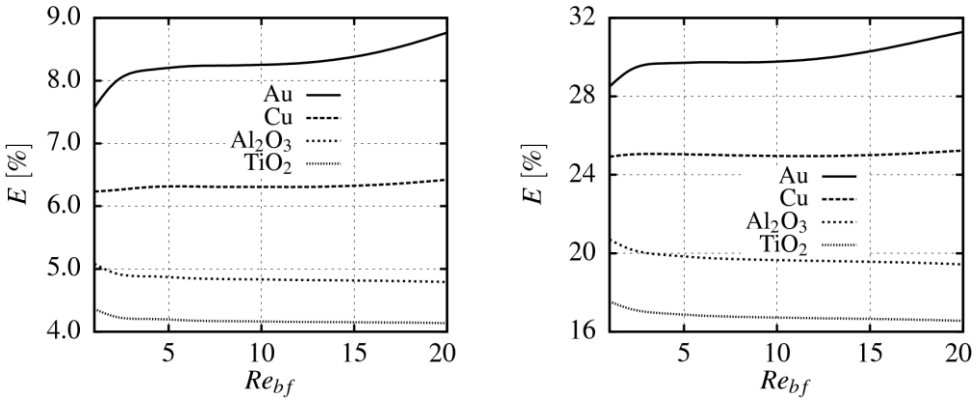

Figure 7: Enhancement of the heat transfer rate for water-based nanofluids at $\varphi = 2{,}5$ % (left) and $\varphi = 10$ % (right).

Last but not least, water-based Au and Cu nanofluid is characterized with the highest heat transfer rate enhancement. However, in spite of lower mean Nusselt number values, Al_2O_3 water-based nanofluid yields greater heat transfer rate enhancement than TiO_2 water-based nanofluid, due to the higher ratio of the nanofluid to the base fluid thermal conductivity k_{nf}/k_{bf}.

6. CONCLUSIONS

In the present study, steady and laminar forced convection of water-based nanofluids from an unconfined circular cylinder has been investigated by numerical means. Governing equations have been solved by the standard finite volume method on the non-uniform Cartesian grid for the range of the base-fluid Reynolds number ($1 \leq Re_{bf} \leq 20$) and volume fraction of nanoparticles ($0\ \% \leq \varphi \leq 10\ \%$).

The influence of computational grid refinement on the present numerical predictions was studied throughout the examination of grid convergence for water-based Au nanofluid at $Re_{bf} = 20$ and $\varphi = 0$ %. By utilizing extremely fine meshes the resulting discretisation error for the mean Nusselt number is reduced below 0,1 %.

Numerical method was validated for the case of the forced convection in Newtonian fluid from heated circular cylinder, for which the results are available in an open literature. Remarkable agreement of present results with the benchmark results yields sufficient confidence in present numerical procedure and results.

Highly accurate numerical results revealed some important points such as:

- Addition of nanoparticles to the base-fluid decreases the nanofluid Prandtl number values and increases the thermal diffusivity.

- Increase in thermal diffusivity causes the reduction in the temperature gradients and, accordingly, increases the thermal boundary thickness. Finally, this increase in the thermal boundary layer thickness reduces the local as well as the mean Nusselt number values.
- The mean Nusselt number $\overline{Nu}$ monotonically increases with increasing base-fluid Reynolds number Re_{bf} but the mean Nusselt number values obtained for the higher values of the nanoparticles' volume fraction are smaller than those obtained in the case of the pure base-fluid at the same nominal values of the base fluid Reynolds number.
- Enhancement of the heat transfer rate E increases with increasing solid volume fraction φ.
- Nanoparticles having the higher ratio k_{nf} / k_{bf} yield greater enhancement of heat transfer rate.

7. ACKNOWLEDGEMENTS

The research leading to these results was carried out within the framework of a research project "Production technology of Au nano-particles" (L2-4212) and has received funding from the Slovenian Research Agency (ARRS).

REFERENCES

[1] Sitek, L.; Foldyna, J.; Martinec, P.; Klich, J.; Maslan, M. (2012). On the preparation of precursors and carriers of nanoparticles by water jet technology, *Technical Gazette*, Vol. 19, No. 3, 465-474

[2] Goktepe, S.; Atalik, K.; Erturk, H. (2014). Comparison of single and two-phase models for nanofluid convection at the entrance of a uniformly heated tube, *International Journal of Thermal Sciences*, Vol. 80, 83-92, doi:10.1016/j.ijthermalsci.2014.01.014

[3] Vukcevic, V.; Werner, A.; Degiuli, N. (2012). Application of smoothed particle hydrodynamics method for simulating incompressible laminar flow, *Transactions of FAMENA*, Vol. 36, No. 4, 1-12

[4] Hadziahmetovic, H.; Hodzic, N.; Kahrimanovic, D.; Dzaferovic, E. (2014). Computational fluid dynamics (CFD) based erosion prediction model in elbows, *Technical Gazette*, Vol. 21, No. 2, 275-282

[5] Rek, Z.; Rudolf, M.; Zun, I. (2012). Application of CFD simulation in the development of a new generation heating oven, *Strojniski vestnik – Journal of Mechanical Engineering*, Vol. 58, No. 2, 134-144, doi:10.5545/sv-jme.2011.163

[6] Venko, S; Vidrih, B.; Pavlovic, E.; Medved, S. (2012). Enhanced heat transfer on thermo active cooling wall, *Strojniski vestnik – Journal of Mechanical Engineering*, Vol. 58, No. 11, 623-632, doi:10.5545/sv-jme.2012.436

[7] Khanafer, K.; Vafai, K.; Lightstone, M. (2003). Buoyancy-driven heat transfer enhancement in a two-dimensional enclosure utilizing nanofluids, *International Journal of Heat and Mass Transfer*, Vol. 46, No. 19, 3639-3653, doi:10.1016/S0017-9310(03)00156-X

[8] Abu-Nada, E.; Oztop, H. F. (2009). Effects of inclination angle on natural convection in enclosures filled with Cu–water nanofluid, *International Journal of Heat and Fluid Flow*, Vol. 30, No. 4, 669-678, doi:10.1016/j.ijheatfluidflow.2009.02.001

[9] Putra, N.; Roetzel, W.; Das, S. K. (2003). Natural convection of nano-fluids, *Heat and Mass Transfer*, Vol. 39, No. 8-9, 775-784, doi:10.1007/s00231-002-0382-z

[10] Ternik, P.; Rudolf, R.; Zunic, Z. (2013). Numerical study of Rayleigh-Benard natural-convection heat-transfer characteristics of water-based Au nanofluids, *Materials and Technology*, Vol. 47, No. 2, 211-215

[11] Ternik, P.; Rudolf, R. (2014). Conduction and convection heat transfer characteristics of water-based Au nanofluids in a square cavity with differentially heated side walls subjected to constant temperatures, *Thermal Science*, Vol. 18, Suppl. 1, 189-200, doi:10.2298/TSCI130604082T

[12] Valipour, M. S.; Ghadi, A. Z. (2011). Numerical investigation of fluid flow and heat transfer around a solid circular cylinder utilizing nanofluid, *International Communications in Heat and Mass Transfer*, Vol. 38, No. 9, 1296-1304, doi:10.1016/j.icheatmasstransfer.2011.06.007
[13] Etminan-Farooji, V.; Ebrahimnia-Bajestan, E.; Niazmand, H.; Wongwises, S. (2012). Unconfined laminar nanofluid flow and heat transfer around a square cylinder, *International Journal of Heat and Mass Transfer*, Vol. 55, No. 5-6, 1475-1485, doi:10.1016/j.ijheatmasstransfer.2011.10.030
[14] Sarkar, S.; Ganguly, S.; Biswas, G. (2012). Mixed convective heat transfer of nanofluids past a circular cylinder in cross flow in unsteady regime, *International Journal of Heat and Mass Transfer*, Vol. 55, No. 17-18, 4783-4799, doi:10.1016/j.ijheatmasstransfer.2012.04.046
[15] Urevc, J.; Koc, P.; Stok, B. (2011). Characterization of material parameters used in the mathematical modelling of arc welding and heat treatment processes, *Transactions of FAMENA*, Vol. 35, No. 4, 1-14
[16] Rahimi, M.; Hosseini, M. J.; Barari, A.; Domairry, G.; Ebrahimpour, M. (2011). Analytical evaluation of heat transfer conductivity with variable properties, *Technical Gazette*, Vol. 18, No. 3, 315-320
[17] Petkovsek, G.; Dzebo, E.; Cetina, M.; Zagar, D. (2010). Application of non-discrete boundaries with friction to smoothed particle hydrodynamics, *Strojniski vestnik – Journal of Mechanical Engineering*, Vol. 56, No. 5, 307-315
[18] Neslusan, M.; Mrkvica, I.; Cep, R.; Raos, P. (2012). Heat distribution when nickel alloy grinding, *Technical Gazette*, Vol. 19, No. 4, 947-951
[19] Hsu, F. H.; Wang, K.; Huang, C. T.; Chang, R. Y. (2013). Investigation on conformal cooling system design in injection molding, *Advances in Production Engineering & Management*, Vol. 8, No. 2, 107-115, doi:10.14743/apem2013.2.158
[20] Versteeg, H. K.; Malalasekera, W. (1995). *An Introduction to Computational Fluid Dynamics: The Finite Volume Method*, Addison Wesley Longman Ltd., Harlow
[21] Patankar, S.V. (1980). *Numerical Heat Transfer and Fluid Flow*, Hemisphere Publishing Corporation, Taylor & Francis Group, New York
[22] Weller, H. G.; Tabor, G.; Jasak, H.; Fureby, C. (1998). A tensorial approach to computational continuum mechanics using object-oriented techniques, *Computers in Physics*, Vol. 12, 620-631, doi:10.1063/1.168744
[23] Patankar, S.V.; Spalding, D. B. (1972). A calculation procedure for heat, mass and momentum transfer in three-dimensional parabolic flows. *International Journal of Heat and Mass Transfer*, Vol. 15, No. 10, 1787-1806, doi:10.1016/0017-9310(72)90054-3
[24] Shyy, W.; Thakur, S.; Wright, J. (1992). Second-order upwind and central difference schemes for recirculating flow computation, *American Institute of Aeronautics and Astronautics Journal*, Vol. 30, No. 4, 923-932, doi:10.2514/3.11010
[25] Ternik, P.; Rudolf, R. (2012). Heat transfer enhancement for natural convection flow of water-based nanofluids in a square enclosure, *International Journal of Simulation Modelling*, Vol. 11, No. 1, 29-39, doi:10.2507/IJSIMM11(1)3.198
[26] Ternik, P.; Rudolf, R. (2013). Laminar natural convection of non-Newtonian nanofluids in a square enclosure with differentially heated side walls, *International Journal of Simulation Modelling*, Vol. 12, No. 1, 5-16, doi:10.2507/IJSIMM12(1)1.215
[27] Ternik, P.; Rudolf, R.; Zunic, Z. (2012). Numerical study of heat transfer enhancement of homogeneous water-Au nanofluid under natural convection, *Materials and Technology*, Vol. 46, No. 3, 257-261
[28] Bilus, I.; Morgut, M.; Nobile, E. (2013). Simulation of sheet and cloud cavitation with homogenous transport models, *International Journal of Simulation Modelling*, Vol. 12, No. 2, 94-106, doi:10.2507/IJSIMM12(2)3.229
[29] Bharti, R. P.; Chhabra, R. P.; Eswaran, V. (2007). Steady forced convection heat transfer from a heated circular cylinder to power-law fluids, *International Journal of Heat and Mass Transfer*, Vol. 50, No. 5-6, 977-990, doi:10.1016/j.ijheatmasstransfer.2006.08.008
[30] Soares, A. A.; Ferreira, J. M.; Chhabra, R. P. (2005). Flow and forced convection heat transfer in crossflow of non-Newtonian fluids over a circular cylinder, *Industrial & Engineering Chemistry Research*, Vol. 44, No. 15, 5815-5827, doi:10.1021/ie0500669